ISSN: 0975-833X

Available online at http://www.journalcra.com

International Journal of Current Research
Vol. 16, Issue, 06, pp.28822-28829, June, 2024
DOI: https://doi.org/10.24941/ijcr.47323.06.2024

INTERNATIONAL JOURNAL OF CURRENT RESEARCH

RESEARCH ARTICLE

THE BEST EFFICIENCY OF ORGANIC-INORGANIC QUANTUM DOTPEROVSKITE SOLAR CELLS

Dhuha Emad Tarek[1], Murtadha Jameel Edam[2,*], Hawraa Mohammed Khadier[3] and Samir Mahdi Abdul Almohsin[2]

[1]Department of Biomedical Engineering, College of Engineering, University of Thi-Qar, Thi-Qar, 64001, Iraq,
[2]Department of Physics, College of Education for Pure Sciences, University of Thi-Qar, Thi-Qar, 64001, Iraq,
[3]Department of Physics, College of Sciences, University of Thi-Qar, Thi-Qar, 64001, Iraq,

ARTICLE INFO

Article History:
Received 20th March, 2024
Received in revised form
15th April, 2024
Accepted 24th May, 2024
Published online 30th June, 2024

Key words:
Quantum Dot, Perovskites, Solar Cells, High-Efficiency.

***Corresponding author:**
Murtadha Jameel Edam

ABSTRACT

Hybrid inorganic–organic perovskites have emerged over the last 5 years as a promising class of materials for optoelectronic applications. Most notably, their solar cells have achieved power conversion efficiencies above 20% in an unprecedented timeframe, A theoretical investigation into Quantum dot (QD) nanocrystals have been proposed for high-efficiency solar cells due to their exceptional qualities, and this research is focused on examining the quantum efficiency of perovskites. Perovskites / ZnSe Assuming that QDs have the geometry of a quantum disk assuming n and p perovskites/ETL as QD layers.

Citation: Dhuha Emad Tarek, Murtadha Jameel Edam, Hawraa Mohammed Khadier and Samir Mahdi Abdul Almohsin. 2024. "The best efficiency of organic-inorganic quantum dotperovskite solar cells*". International Journal of Current Research*, 16, (06), 28822-28829.

INTRODUCTION

Zerodimensional crystals (QD) have gotten a lot of attention because of their remarkable electrical and optical properties. The influence of quantum confinement on electrons should be investigated first, followed by the notion of QDs. Quantum confinement occurs when one or more crystal sizes exceed the exciton Bohr radius. The notions of energy levels, bandgaps, conduction, and valence bands remain relevant. In the quantum well (QW), the electron has at least two degrees of freedom, but only one degree in the quantum wire (shown in figure1). Despite shifting the state density in 1D or 2D energy sub-bands, this type of confinement allows the electron to go in one direction. QDs are materials having discrete building units ranging from 1 to 100 nm in size. QDs are referred to be artificial atoms because, unlike naturally occurring atoms or molecules, they have limited, distinct electronic states [1].Due to its unique qualities, such as an adjustable band gap and an innately high absorption coefficient, quantum dots (QDs) have been increasingly popular in photovoltaics in recent years. generation of multiple exciton[2]**.** In order to build efficient solar cells sensitized with perovskite QDs, we propose using the perovskite QD/ETL composite. It can be created using a disk model.

Theoretical Model: Figure 2 shows a schematic representation of a quantum disk in cylindrical dimensions. The energy levels of the quantum disk are determined by solving the Schrödinger equation in the parabolic band model. This model is used to determine energy levels in the conduction band (CB) and valence band (VB) for the structures studied (VB).

Model of a Quantum Disk

The Schrödinger equation in cylindrical dimensions (ρ, φ, z) for a quantum disk with radius (ρ) and height (h) is

$$\left\{-\frac{\hbar^2}{2m^*}\left[\nabla^2+V\right]\right\}\psi(\rho,\varphi,z)=E\,\psi(\rho,\varphi,z) \tag{1}$$

$$\left\{-\frac{\hbar^2}{2m^*}\left[\nabla^2+V\right]\right\}\psi(\rho,\varphi,z)=E\,\psi(\rho,\varphi,z) \tag{2}$$

There are three sections to the wave function Ψ :

$$\Psi(\rho,\varphi,z)=R(\rho)\Phi(\varphi)Z(z) \tag{3}$$

Where ρ , φ and Z are appearing in Fig. 2.1. Substituting Eq. (3) into Eq. (1), and dividing by $R\,\Phi Z$ to get,

$$-\frac{\hbar^2}{2m^*}\left[\frac{1}{R}\frac{1}{\rho}\frac{\partial}{\partial\rho}\left(\rho\frac{\partial R}{\partial\rho}\right)+\frac{1}{\Phi}\frac{1}{\rho^2}\frac{\partial^2\Phi}{\partial\varphi^2}+\frac{1}{Z}\frac{\partial^2 Z}{\partial z^2}\right]=(E-V)R\,\Phi\,Z \tag{4}$$

The only term in Eq. (4) that is a function of (z) is the final term, whereas the other ones are not. Separating the components of this equation that are dependent on R , φ , and z We have a solution for the wave function of the form by equating the z -component to a constant p , then utilizing the wave function's boundary conditions (BCs) and the fact that it is the first derivative.

$$Z(z)=\begin{cases}C_1\cos(p\,z), & |z|<\frac{h}{2}\\ C_2 e^{-\alpha\left(|z|-\frac{h}{2}\right)}, & |z|\geq\frac{h}{2}\end{cases} \tag{5}$$

Where

$$p=\frac{\sqrt{2m_d^*(E_z-V_d)}}{\hbar}\quad\text{and}\quad q=\frac{\sqrt{2m_b^*(V_b-E_z)}}{\hbar} \tag{6}$$

Now substituting Eq. (5) into Eq. (4), and multiply by ρ2 will lead to,

$$\frac{\rho}{R}\frac{\partial}{\partial\rho}\left(\rho\frac{\partial R}{\partial\rho}\right)+\frac{1}{\Phi}\frac{\partial^2\Phi}{\partial\varphi^2}+p^2\rho^2=0 \tag{7}$$

$$\rho\frac{\partial}{\partial\rho}\left(\rho\frac{\partial R}{\partial\rho}\right)+\left(p^2\rho^2-m^2\right)R=0 \tag{8}$$

This equation has a solution $J_m(\rho p)$, and $K_m(qp)$ the Bessel functions of the first and second class are the solutions. The genesis of the second K_m sort differs from the first. As a result, it can't be utilized everywhere. As a result, the Bessel function is $J_P(\alpha x)$ the solution of Eq. (9).

$$R(\rho)=\begin{cases}C_1J_m(p\rho) & \rho\leq a\\ C_1K_m(q\rho) & \rho>a\end{cases} \tag{9}$$

In the ρ-φ direction, we have a solution of the form

$$\psi(\rho,\varphi)=\frac{e^{im\varphi}}{\sqrt{2\pi}}\begin{cases}C_1J_m(\rho p) & \rho\leq a\\ C_2K_m(qp) & \rho>a\end{cases} \tag{10}$$

The constants p and q have the relationship after some mathematical modification of the appropriate wave equation in the dot and the barrier[6].

$$(pa)^2 + \frac{m_d^*}{m_b^*}(qa)^2 = \frac{2m_d^*(V_b - V_d)a^2}{\hbar^2} \tag{11}$$

The effective mass $m^* = m_d$ inside the disk and $m^* = m_b$ in the barrier. Similarly, the electric potential is $V = V_d$ inside the disk and $V = V_b$ in the barrier.

$$V(z) = \begin{cases} V_b, & |z| \geq \frac{h}{2} \\ 0, & |z| < \frac{h}{2} \end{cases} \tag{12}$$

In general, the solutions for quantized eigenenergies may be derived directly from the graphical solution by obtaining (L/2) and (p L/2).

$$(p\frac{h}{2})^2 + \frac{m_d^*}{m_b^*}(\alpha\frac{h}{2})^2 = \frac{2m_d^* V_b (\frac{h}{2})^2}{\hbar^2} \tag{13}$$

and

$$\alpha'\frac{h}{2} = \sqrt{\frac{m_b}{m_d}}\, p\frac{h}{2}\tan(p\frac{h}{2}) \quad \text{Even solution} \tag{13-a}$$

$$\alpha'\frac{h}{2} = -\sqrt{\frac{m_b}{m_d}}\, p\frac{h}{2}\cot(p\frac{h}{2}) \quad \text{Odd solution} \tag{13-b}$$

Plotting the aforementioned equations on the ($\alpha'\frac{h}{2}$, $p\frac{h}{2}$) plane allows them to be solved.

Eq. (13) represents a radiuses circle $\sqrt{2m_d^* V_b}\,(h/2\hbar)$.

The solutions to α' and p are obtained from the intersections between the circle (2.31) and either of the curves (13-a), (13-b). The transverse Eigen energy E_ρ is derived by setting the disk potential to Vd = 0[6].

$$E_\rho = \frac{\hbar^2}{2m_d^*}\frac{(pa)^2}{a^2} \tag{14}$$

The longitudinal eigenenergy Ez is calculated as follows:

$$E_z = \frac{\hbar^2}{2m_d^*}\frac{\left(p\frac{h}{2}\right)^2}{\left(\frac{h}{2}\right)^2} \tag{15}$$

The quantum disk's total eigenenergy The total of the transverse and longitudinal eigenenergies is Ed, which is written as:

$$E_d = E_\rho + E_z \tag{16}$$

Absorption coefficients: Photons emitted by QDs have somewhat different energy than photons emitted by transition states. The non-homogeneous broadening is caused by defects in the shape and distribution of QDs. As a result, the absorption coefficient is expressed as

$$\alpha(\hbar\omega) = \frac{\pi e^2}{n_b c \varepsilon_o \omega m_o^2} \sum_i \int_{-\infty}^{\infty} dE' |M_{env}|^2 |\hat{e} P_{cv}|^2 D(E') L_g(E', \hbar\omega)$$
$$[f_v(E', F_v) - f_c(E', F_c)] \quad (17)$$

where m_0 is themass of free electron mass, ε_0 is permittivity of free space, c is speed of light, and n_b is refractive index, ω is the injected optical signal's angular frequency, E' is the optical transition energy, and $|M_{env}|^2$ is the envelope function that overlaps the QD electron and hole states.The optical matrix energy parameter , $|\hat{e}.P_{cv}|^2 = \frac{3}{2}(m_0/6)E_p$ is the momentum matrix element for electron-heavy hole transition energy in TE polarization E_p. $D(E')$ is the self-assembled QDs' inhomogeneous density of states, and it's written as [5].

$$D(E') = \frac{s^i}{V_{dot}^{eff}} \frac{1}{\sqrt{2\pi\sigma^2}} \exp\left(\frac{-(E' - E_{max}^i)^2}{2\sigma^2}\right) \quad (18)$$

Where s^i is the degeneracy number for both the ground state and the excited state of the QD, respectively.V_{dot}^{eff} is the effective volume of QDs, σ is the spectral variance of the QD distribution, and E_{max}^i is the optical transition transition energy at the maximum of the QD distribution of the i^{th} optical transition. Bands of conduction and valence, the terms f_c and f_v are the corresponding quasi-Fermi distribution functions. The term "world condition" has been employed to characterize characterize the quasi-Fermi conduction levels on a global scale and F_v bands of valence, which comprise contributions from the barrier layer and WL as well as QDs. The density of surface carriers per QD layer may be calculated as follows [5]:

$$n_{2D} = N_D \sum_i \frac{s^i}{\sqrt{2\pi\sigma_e^2}} \int dE_c' e^{-(E_c' - E_{ci})/2\sigma_e^2} f_c(E_c', F_c) + \sum_l \frac{m_e^* K_B T}{\pi\hbar^2} \ln(1 + e^{(F_c - E_{cl})/K_B T})$$
$$+ \tau_b \frac{1}{2\pi^2} \left(\frac{2K_B T m_{eb}^*}{\hbar^2}\right)^{\frac{3}{2}} e^{\left(\frac{F_c - E_{cb}}{K_B T}\right)} \quad (19\text{-a})$$

$$p_{2D} = n_{2D} + N_A^-$$
$$p_{2D} = N_D \sum_i \frac{s^i}{\sqrt{2\pi\sigma_h^2}} \int dE_h' e^{-(E_h' - E_{hi})/2\sigma_h^2} f_v(E_h', F_v) + \sum_m \frac{m_{hh}^* K_B T}{\pi\hbar^2} \ln(1 + e^{(F_V - E_{vm})/K_B T})$$
$$+ \tau_b \frac{1}{2\pi^2} \left(\frac{2K_B T m_{hhb}^*}{\hbar^2}\right)^{\frac{3}{2}} e^{\left(\frac{F_V - E_{hhb}}{K_B T}\right)} \quad (19\text{-b})$$

Where n_{2D} and p_{2D} are the electron and hole surface densities per QD layer, respectively. The terms E_c' and E_h' reflect the respective restricted QD state in the conduction and valence bands, E_{ci} and E_{hi} are the energy in the conduction band and the energy in the valence band, respectively. The spectrum σ_e and σ_h variance of the electron and heavy hole distributions in a quantum dot, is $m_e^*(m_{hh}^*)$ and $E_{cl}(E_{vm})$ The variables and are the effective electron (hole) mass and sub band edge energy of WL's conduction (valence) band, respectively. The word τ_b refers to the thickness of the QD's barrier layer.The words $m_{eb}^*(m_{hhb}^*)$ and $E_{cb}(E_{hhb})$ refer to the barrier layer's Conduction (valence) band edge energy and effective electron (hole) mass. The absorption coefficient's Lorentzian line shape function $L_g(E', \hbar\omega)$ is given by [5]

$$L_g(E', \hbar\omega) = \frac{1}{\sqrt{2\pi\sigma^2}} \exp\left(\frac{-(E' - \hbar\omega)^2}{2\sigma^2}\right) \quad (20)$$

Quantum Efficiency in Quantum Dot Solar Cells Calculation

The generating rate was expressed on the p-side. as follows[5]:

$$G(x) = (1-R)\alpha_n \phi \exp\{-(\alpha_n x_j + \alpha_d W + \alpha_p [x - x_j - W]) \quad (21)$$

Where R is the optical reflectivity between the air and the semiconductor, Φ is the illuminated photon number, $\alpha_p, \alpha_n, \alpha_d$ are the absorption coefficients of $p-$, $n-$ the depletion layers, respectively, x_j is the depletion depth, and W is the depletion width. The extra hole density in the $n-$ side has a relationship that is provided by[7]

$$\delta p_n = \frac{\alpha_n \phi(1-R)\tau_p}{(\alpha_n^2 L_p^2 - 1)} \left\{ \frac{\cosh(x/L_p)}{\sinh(x_j/L_p)} \left[-\frac{(D_p \alpha_n^2 - S_p)}{(D_p/L_p^2 - S_p)} e^{(x_j/L_p)} + e^{-\alpha_n x_j} \right] + \frac{(D_p \alpha_n^2 - S_p)}{(D_p/L_p^2 - S_p)} e^{(x/L_p)} - e^{-\alpha_n x} \right\} \tag{22}$$

S_p is the layer's surface recombination velocity

L_p is the length of the hole diffusion, $L_p = \sqrt{\tau_p D_p}$

D_p is the hole's diffusion coefficients

The diffusion dominates the hole diffusion photo current in the side, which is given by [7].

$$J_p \approx -qD_p \frac{\partial}{\partial x} \delta p_n \tag{23}$$

To obtain, use Eq. (2.41),

$$J_p = \frac{qL_p \alpha_n \phi (1-R)}{(\alpha_n^2 L_p^2 - 1)} \left\{ \coth(x_j/L_p) \left[\frac{(D_p \alpha_n^2 - S_p)}{(D_p/L_p^2 - S_p)} e^{x_j/L_p} - e^{-\alpha_n x_j} \right] + \frac{(D_p \alpha_n^2 - S_p)}{(D_p/L_p^2 - S_p)} e^{x_j/L_p} - \alpha_n L_p e^{-\alpha_n x_j} \right\} \tag{24}$$

The excess electron density in the side has the following relationship:

$$\delta n_p(x) = \frac{\alpha_p \phi(1-R)\tau_n}{(\alpha_p^2 L_n^2 - 1)} e^{-(\alpha_n x_j - \alpha_d W)} \left\{ e^{-(x - x_j - W/L_n)} + \frac{\sinh(x - x_j - W/L_n)}{\sinh(H'/L_n)} \left[\frac{D_n}{L_n^2} - S_n \right] \left[(\alpha_p^2 - S_n) e^{-\alpha_p H} - ([D_n/L_n^2] - S_n) e^{-\frac{H'}{L_n}} - e^{-\alpha_p (x - x_j - W)} \right] \right\} \tag{25}$$

The diffusion dominates the electron diffusion photo current in the side, which is given by

$$J_n = qD_n \frac{\partial}{\partial x} \delta n \tag{26}$$

The electron current density, on the other hand, may be expressed as:

$$J_n = q \frac{\phi \alpha_p L_n (1-R)}{(\alpha_p^2 L_n - 1)} e^{-(\alpha_n x_j + \alpha_d W)} \times \left\{ \frac{(\alpha_p^2 - S_n) L_n^2}{(D_n - S_n L_n^2)} e^{-\alpha_p H'} - 2e^{-\frac{H'}{L_n}} + \alpha_p L_n e^{-\alpha_p H'} \right\} \tag{27}$$

The depletion region's drift photocurrent is calculated as follows:

$$J_{dr} = q\phi(1-R) e^{-\alpha_n x_j} (1 - e^{-\alpha_d W}) \tag{28}$$

It's worth noting that the QE of QD Solar Cells is calculated as follows:

$$QE = \frac{(J_p + J_n + J_{dr})}{q\phi(1-R)} \tag{29}$$

RESULTS AND DISCUSSION

$CH_3NH_3PbBr_3$ / Zn Seperoviskite Quantum dot

It has a wavelength range of 240-270nm, which is in the UV spectrum. Three peaks have developed in the curve at 213 k. The first one, which derives from the 1 to 5th subband transitions, is at 251nm. The second peak, at 254nm, is caused by subband transitions from 2 to 2. The 1 to 1 subband transitions give rise to the third peak at 255nm.Three peaks have developed in the curve at 273 K. The first is at 249nm, which is caused by transitions from the third to fourth subbands. The second peak, at 253nm, is caused by transitions from the first to fourth subbands. The 1 to 2 subband transitions produce the third peak, which is located at 254nm. Three peaks have developed in the curve at 333 K. The first is at 245nm, which is caused by transitions between the 2nd and 5th subbands. The 1 to 5th subband transitions give rise to the second peak at 251nm. The transitions between the 2nd and 4th subbands produce the third peak at 253nm. As the temperature rises, so does the absorption and quantum efficiency.as fig 4

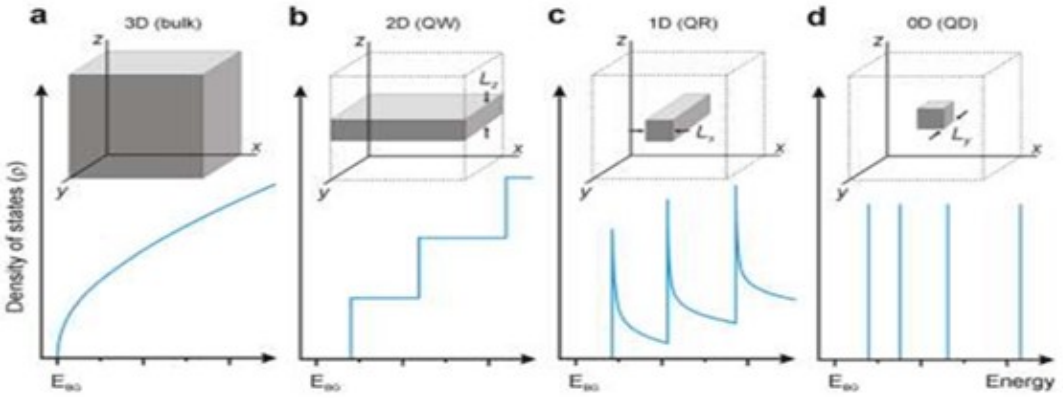

Figure 1. Density of states in bulk and quantized structures: (a) bulk; (b) quantum well (QW) structure; (c) quantum wire (QR) structure; and (d) quantum dot (QD) structure[3].

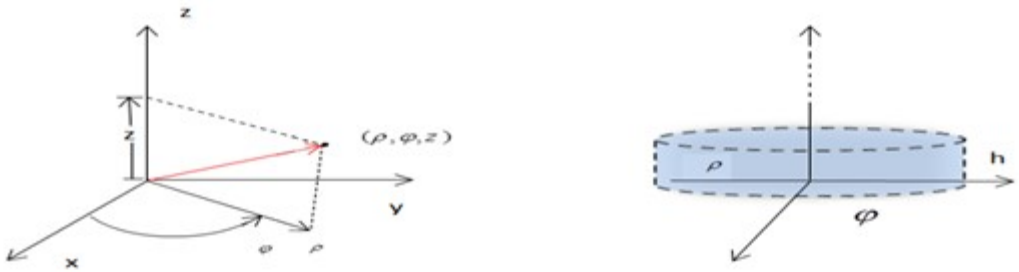

Figure 2. A schematic representation of the quantum disk with cylindrical dimensions [4]**.**

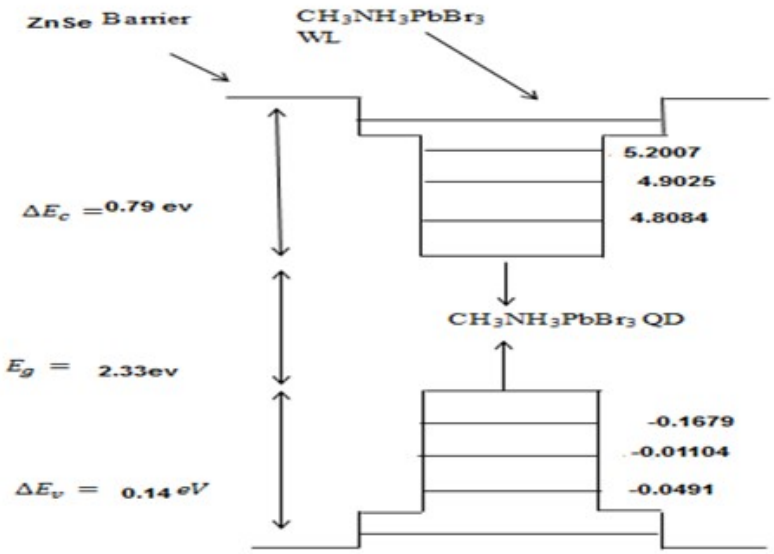

Figure 3. Energy band diagram of the $CH_3NH_3PbBr_3$/ZnSe QD structure

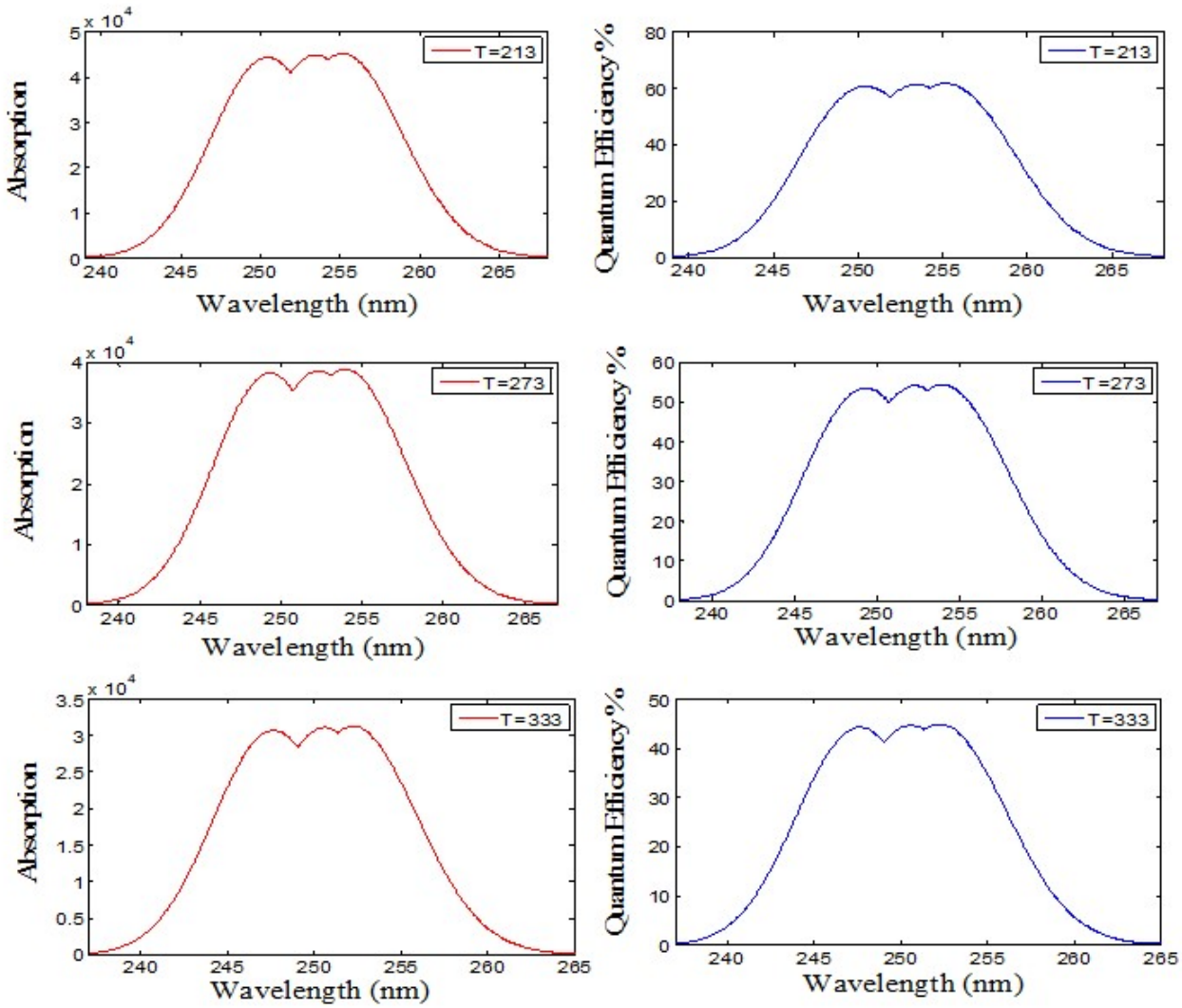

Table 1. Material parameters

Parameter	Symbol	CH3NH3PbBr3(Q-D)	ZnSe
Energy gap	E_g	2.33 eV	1.4 eV
Electron effective mass	m^*_e	0.5 m_0	0.2 m_0
Hole effective mass	m^*_h	0.23 m_0	0.6 m_0
Refractive index	n_b	2.29	
Conduction band offset	ΔE_c	0.79 eV	
Valence band offset	ΔE_v	0.14 eV	
CB-QD energy level	4.8084 ,4.9025 ,5.2007 ,5.4506 ,5.5447		
VB-QD energy levels	-0.0491 ,-0.1104 ,-0.1679, -0.2436		

CONCLUSION

This work deals to study the Absorption coefficient and Quantum Efficiency of $CH_3NH_3PbBr_3$/ZnSe, QD Solar cells. These structures cover the range of (240-270) nm in the emission spectrum. To predict their Solar cells characteristics, their band QD structures were calculated assuming the quantum disk shape. this calculate with change the temperatures. When increasing the temperature leads to decrease the Absorption coefficient and Quantum Efficiency.

REFRENCES

Im, J. H. C.-R. Lee, J.-W. Lee, S.-W. Park, and N.-G. Park, "6.5% efficient perovskite quantum-dot-sensitized solar cell," *Nanoscale*, vol. 3, no. 10, pp. 4088–4093, 2011.

Zeng X. *et al.*, "Performance improvement of perovskite solar cells by employing a CdSe quantum dot/PCBM composite as an electron transport layer," *J. Mater. Chem. A*, vol. 5, no. 33, pp. 17499–17505, 2017.

Ray S. S. and M. Okamoto, "Polymer/layered silicate nanocomposites: a review from preparation to processing," *Prog. Polym. Sci.*, vol. 28, no. 11, pp. 1539–1641, 2003.

Kirchmeyer S. and K. Reuter, "Scientific importance, properties and growing applications of poly (3, 4-ethylenedioxythiophene)," *J. Mater. Chem.*, vol. 15, no. 21, pp. 2077–2088, 2005.

Kim J. and S. L. Chuang, "Theoretical and experimental study of optical gain, refractive index change, and linewidth enhancement factor of p-doped quantum-dot lasers," *IEEE J. Quantum Electron.*, vol. 42, no. 9, pp. 942–952, 2006.

Tian J. *et al.*, "Enhanced performance of CdS/CdSe quantum dot cosensitized solar cells via homogeneous distribution of quantum dots in TiO2 film," *J. Phys. Chem. C*, vol. 116, no. 35, pp. 18655–18662, 2012.

Mou, S. J. V Li, and S. L. Chuang, "Quantum efficiency analysis of InAs–GaSb type-II superlattice photodiodes," *IEEE J. Quantum Electron.*, vol. 45, no. 6, pp. 737–743, 2009.

****